BROOKHAVEN NATIONAL LABORATORY

BNL-99897-2013-IR-R1

Irradiation Experiment Conceptual Design Parameters for NBSR Fuel Conversion

N. Brown, J-S Baek, A. Hanson, A. Cuadra,
L-Y Cheng, D. Diamond

May 2014

Nuclear Science & Technology Department

Brookhaven National Laboratory

U.S. Department of Energy
National institute of Science & Technology

DISCLAIMER

BNL-99897-2014-IR-R1

Irradiation Experiment Conceptual Design Parameters for NBSR Fuel Conversion, Rev. 1

Manuscript Completed:

April 30, 2014

Prepared by:

N. R. Brown, J. S. Baek, A. L. Hanson, A. Cuadra, L-Y. Cheng, and D. J. Diamond

Nuclear Science & Technology Department
Brookhaven National Laboratory
Upton, NY 11973

Prepared for:

National Institute of Standards and Technology
National Nuclear Security Administration

Abstract

It has been proposed to convert the National Institute of Standards and Technology (NIST) research reactor, known as the NBSR, from high-enriched uranium (HEU) fuel to low-enriched uranium (LEU) fuel. The motivation to convert the NBSR to LEU fuel is to reduce the risk of proliferation of special nuclear material. This report is a compilation of relevant information from recent studies related to the proposed conversion using a metal alloy of LEU with 10 w/o molybdenum. The objective is to inform the design of the mini-plate and full-size-plate irradiation experiments that are being planned. This report provides relevant dimensions of the fuel elements, and the following parameters at steady state: average and maximum fission rate density and fission density, fuel temperature distribution for the plate with maximum local temperature, and two-dimensional heat flux profiles of fuel plates with high power densities. The latter profiles are given for plates in both the inner and outer core zones and for cores with both fresh and depleted shim arms (reactivity control devices). A summary of the methodology to obtain these results is presented. Fuel element tolerance assumptions and hot channel factors used in the safety analysis are also given.

Table of Contents

List of Figures

List of Tables

1. Introduction

This report is a compilation of results from studies of the conversion of the National Institute of Standards and Technology (NIST) research reactor, known as the NBSR, to low-enriched uranium (LEU) fuel. The objective of this document is to convey the information requested by the plate irradiation experiment design team at Idaho National Laboratory.

Brookhaven National Laboratory (BNL) has an extensive history of collaboration with NIST regarding the NBSR. BNL performed safety analysis in support of the NBSR license renewal application [1]. More recently, BNL has performed the design work and safety analysis for the LEU conversion of the NBSR. Some relevant results of these studies have been recently documented [2-8].

The following information was requested for the NBSR LEU fuel plate irradiation experiment for the most disadvantageous steady state LEU core condition [9]:

1. Nominal geometry and configuration of the fuel plates and fuel assemblies
   a. Fuel meat thickness
   b. Cladding thickness
   c. Absorber thickness
   d. Fuel assembly configuration
   e. Fuel management scheme
2. Peak local irradiation condition at maximum licensed power
   a. Fission density (fission/cm^3)
   b. Fission rate density (fission/cm^3-s)
   c. Heat flux distribution
   d. Fuel meat and plate surface temperatures

This report is comprised of the following sections:

1. Introduction
2. Geometry of the Fuel Plates, Fuel Elements, and Reactor Core
3. Limiting LEU Power Distribution
4. High Resolution LEU Power Distribution for Element 8-3E
5. Limiting LEU Local Burn-Up and Fission Density
6. Limiting Fuel Temperatures
7. Tolerance Assumptions and Hot Channel Factors in the Safety Analysis

The contents of Section 2 are sourced from References [1-3] and provide the requested information regarding the nominal LEU fuel plate and fuel element geometry. The contents of Section 3 are sourced from References [2–5] and describe the model geometry, nodalization, fission rate density, and heat flux distribution. The heat flux distribution and fission rate density, as presented within this report, are equivalent. Section 4, added in Rev. 1, consists of a power distribution calculation with a fine transverse mesh in the LEU fuel element that features the peak fission rate density. The contents of Section 5, modified in Rev. 2, are sourced from References [5, 6, 7] and describe the average and maximum fission density as calculated utilizing

local burn-up effect studies. Section 6 is primarily sourced from Reference [3] and Reference [8] and presents the thermal hydraulic nodalization and the relevant steady state fuel meat temperature distribution for the LEU core. Section 7, added in Rev. 1 and modified in Rev. 2, presents the geometry and material tolerance assumptions made in the safety analysis and the hot channel statistical analysis as well as the peak local values of fission rate density, fission density, and heat flux with and without uncertainties.

2. Geometry of the Fuel Plates, Fuel Elements, and Reactor Core

The NBSR is a high burn-up, 20 MWt reactor. The moderation and cooling is provided by D_2O, which flows upward through the core from two concentric plena just below the lower grid plate. The NBSR is designed with several unique features that enable low-energy and thermal neutrons to stream through eight radial beam tubes and two cold neutron sources. These features include an unfuelled "gap" in the axial center of the fuel elements, which contains only moderator and structural materials. This gap, which acts to minimize contamination of the streaming low-energy neutrons, is co-located with the beam tubes at the core axial mid-plane. The mid-plane gap is very significant in terms of the NBSR peak local irradiation condition. The axial thermal flux always peaks in the mid-plane gap. Because the axial location of the thermal flux peak is fixed, the fuel that is directly adjacent to the gap experiences both the highest fission rate density and the highest cumulative fission density in the NBSR core.

Another unique feature of the NBSR is the cadmium shim arms (control elements), which traverse the upper-half of the core in a semaphore fashion. During much of a reactor cycle, the shim arms act to suppress the flux in the upper half of the NBSR core. This flux "compression" shifts the peak local irradiation condition to the fuel in the lower half-element that is nearest to the mid-plane gap. A three-dimensional cut-away view of the NBSR vessel internals and reactor core is shown in Figure 1. The mid-plane gap (legend entry 5) and the shim arms (legend entry 2) are both visible in Figure 1. Due to the combined impact of the mid-plane gap and the shim arms, the local cumulative fission density in the NBSR fuel approaches 100% burn-up of fissile nuclides, primarily ^{235}U and ^{239}Pu.

Presently, the NBSR is fueled with high-enriched uranium (HEU) with a nominal ^{235}U enrichment of 93% [1]. The fuel is U_3O_8 in an aluminum powder dispersion that is clad in aluminum alloy (Alloy 6061). Each fuel element is constructed of 17 fuel plates in each upper and lower half (34 plates per fuel element) and is constructed in the Materials Test Reactor (MTR) curved plate geometry. Each plate is 33.02 cm (13 in) long with 27.94 cm (11 in) of fuel and the fuel width is 6.03 cm (2.373 in). The thickness of fuel meat in each plate is 0.0508 cm (0.020 in) for HEU fuel, with a volume of 148 cm^3 (9.05 in^3) of fuel per half-element. There is a 17.78 cm (7 in) gap between the upper and lower fueled regions of the core. In the gap region, the aluminum plates extend one-half inch below and above the fuel so the physical gap is 15.24 cm (6 in). Each HEU fuel element has a mass of 350±3.4 g of ^{235}U. The aluminum cladding is 0.0381 cm (0.015 in) thick on each side. Figure 2 shows the lower and upper fuel plates and the physical gap in a fuel element.

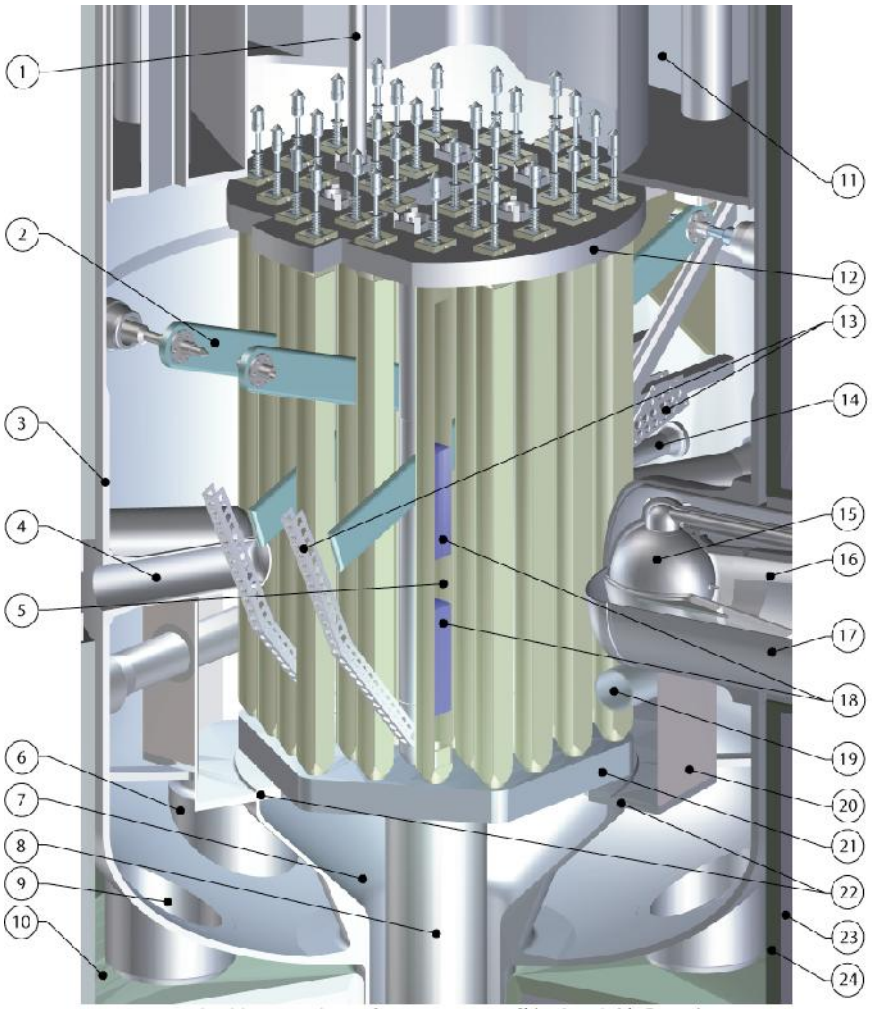

Figure 1 NBSR Vessel Internals and Reactor Core [1]

The fuel meat for the LEU conversion of the NBSR is proposed as U10Mo (10 wt% Mo alloyed with U) metal foils with the same aluminum alloy cladding used in the HEU fuel [2]. The geometrical dimensions of fuel plates in a fuel element are the same for HEU and LEU fuels except for the fuel meat and cladding thickness. Data for the nominal U10Mo fuel design are given in Table 1. The thickness of the LEU fuel foils is 0.0215 cm (0.0085 in) with a total volume of 62.64 cm^3 (3.8 in^3) per half-element. The engineering specification on fuel foil thickness is 0.0085 in. The rolling tolerance of the fuel foils is expected to be ±0.001 in, so the fuel thickness is specified as 0.0085±0.001 in. The ^{235}U content of each LEU fuel element is 383±4 g, where the uncertainty is only due to the uncertainty in the molybdenum content of the LEU fuel. The 10% weight specification for molybdenum has an uncertainty of ±1% (=10%

relative uncertainty). There is also an uncertainty in ^{235}U content due to enrichment uncertainty. The thickness of the aluminum cladding for the LEU fuel is 0.053 cm (0.0208 in) on each side. There is a 0.00254 cm (0.001 in) layer of zirconium between the cladding and the fuel to improve fuel behavior under irradiation and this is also taken into account in the modeling.

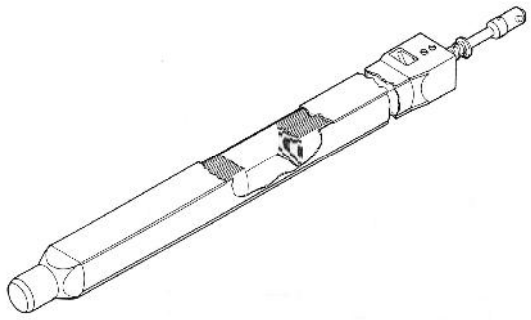

Figure 2 NBSR Fuel Element

Table 1 NBSR Fuel Element Data

Parameter	HEU	LEU
^{235}U grams	350	383
^{238}U grams	26	1556
O grams	68	0
Al grams	625	0
Mo grams	0	215
Total grams	1069	2154
Fuel density (g/cm^3)	3.61	17.2
Fuel meat thickness (cm)	0.0508	0.0215
Fuel volume, half-element (cm^3)	148	62.64

Figure 3 shows a cross sectional view of a fuel element. There are a total of 30 fuel elements in the NBSR core. Six fuel elements are located in the inner core (cooled by flow from the inner plenum) and twenty-four elements in the outer core (cooled by flow from the outer plenum). Figure 4 shows the labeling of fuel element positions. The thimble identifiers are bracketed (< >) and the regulating rod is identified as <RR>. In each position fuel elements are identified with two numbers and one letter. The letters are either E or W for the east or west side of the core noting that a fuel element always stays in the east side or in the west side of the core. The fuel management scheme of the NBSR dictates that 16 fuel elements stay in the core for eight cycles and 14 fuel elements stay in the core for seven cycles. The first number denotes how many cycles the element will be in the core (either eight or seven) and the second number denotes the cycle in which the fuel element resides. Therefore, at the beginning of a cycle, the 8-1 and 7-1 fuel elements are unirradiated fuel elements, whereas 8-8 and 7-7 are in their final cycles and will be removed after the cycle is over. After a cycle is finished the 8-8 and 7-7 fuel elements are removed and the 8-7 elements are moved into the 8-8 positions, the 7-6 elements are moved into the 7-7 positions, etc. The process proceeds until unirradiated fuel is placed in

the 8-1 and 7-1 positions. The reactivity of the NBSR is controlled with four cadmium shim arms that are rotated through the core in a semaphore fashion.

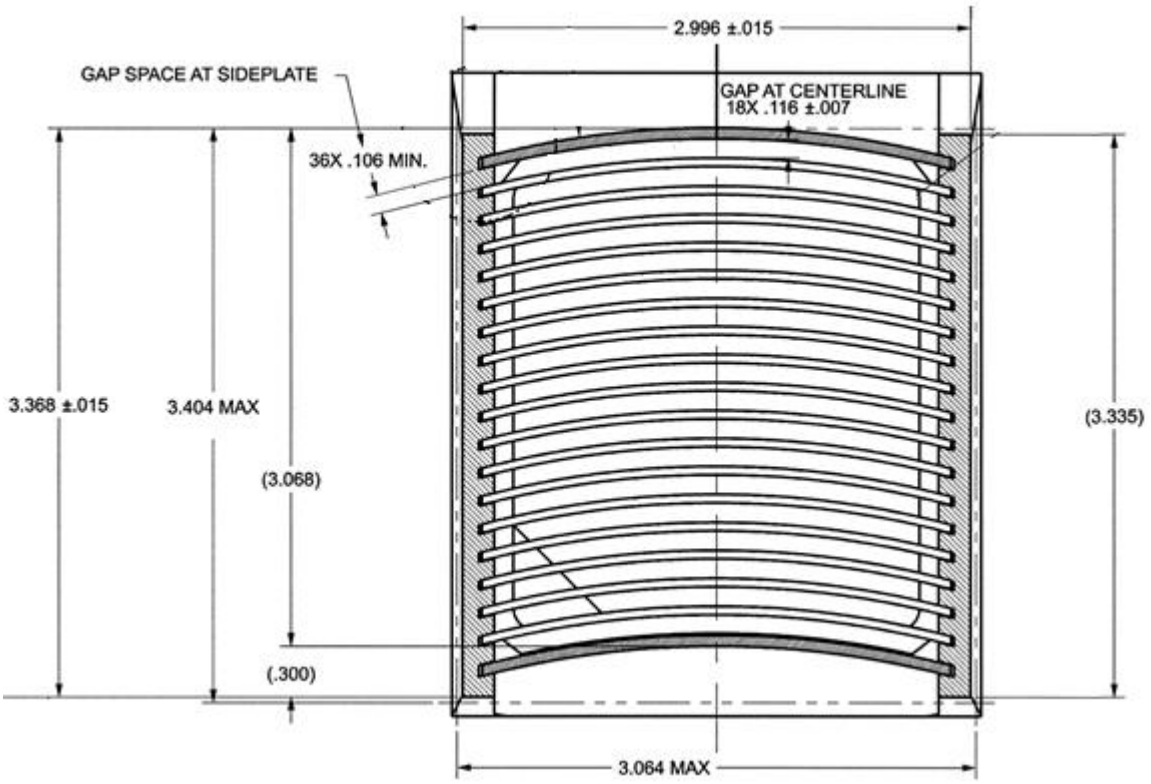

Figure 3 Cross Sectional View of Fuel Element (Dimensions in Inches)

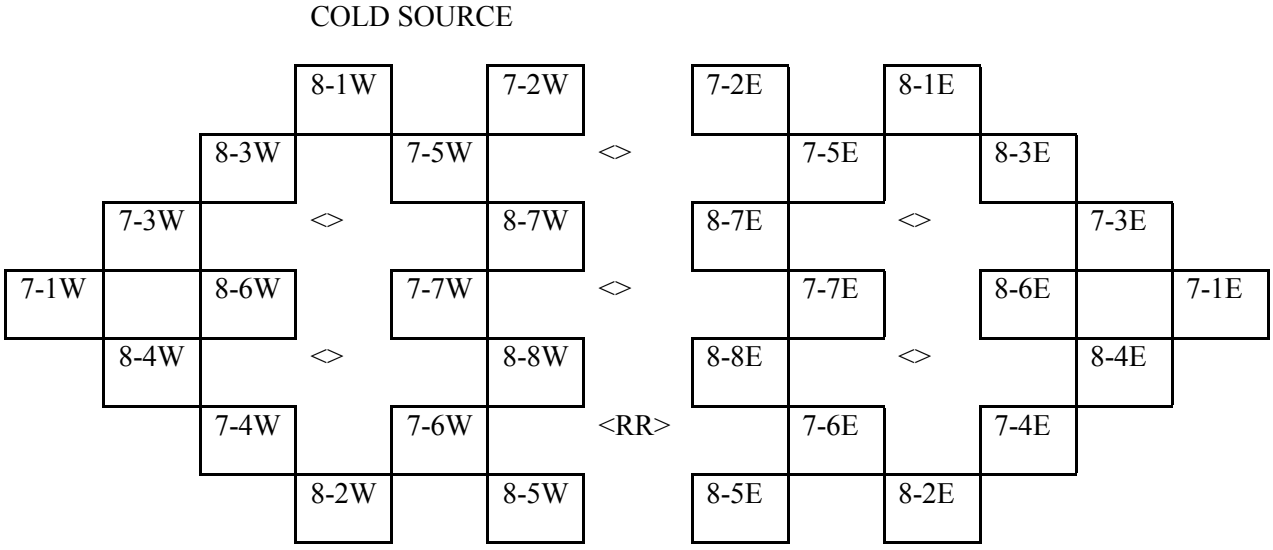

Figure 4 NBSR Fuel Management Scheme

For the conversion of the reactor to LEU fuel, an improved full-core model of the NBSR has been developed (the "present" model) for the neutronic and burn-up analysis [2]. The model utilizes MCNPX [10] to accomplish a detailed burn-up analysis where each half-element has a unique fuel inventory (material composition) that is moved throughout the core for either seven or eight 38.5-day fuel cycles. The NBSR model has been subjected to a variety of validation studies and is an evolution of the model utilized in the NBSR Safety Analysis Report [1]. It has also been utilized to design two cold neutron sources, and to compute the prompt neutron lifetime [2]. A planar view of the NBSR model is shown in Figure 5. Some of the specific improvements made to the burn-up analysis in the present full-core model include [2]:

- reduction in unaccounted mass from ~1.2% per cycle per fuel element to ~0.13% per cycle per fuel element
- increase of the number of isotopes considered from a maximum of 63 to a maximum of 210
- increase of the number of fuel inventories from 30 to 60 eliminating forced symmetry radially, in the half fuel elements' material compositions
- inclusion of the 10.5-day decay time at the end of each cycle
- analysis of additional burn-up state points
- utilization of the ENDF-B/VII.0 cross section libraries
- realistic positioning of the shim arms (control elements) within each burn-up state point

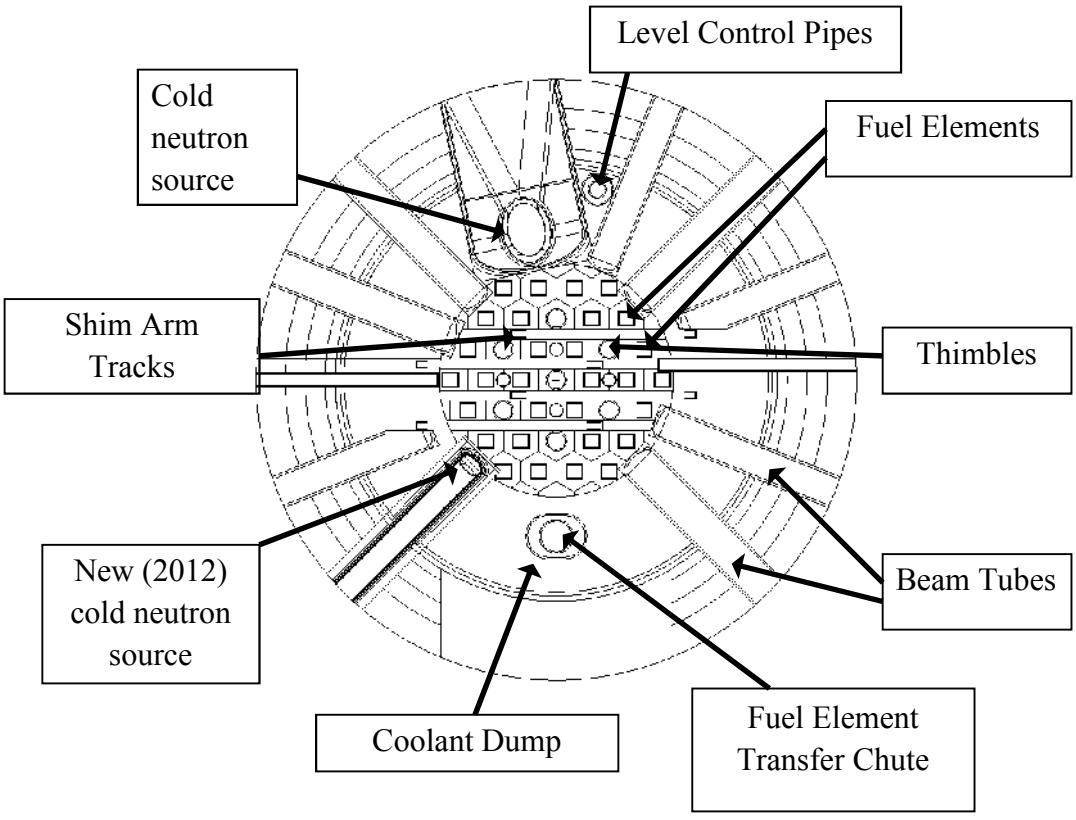

Figure 5 Planar View of the NBSR MCNPX Model

3. Limiting LEU Power Distribution

The purpose of this section is to inform the design and planning of future irradiation experiments by documenting the calculated fission rate density and heat flux distribution in the LEU NBSR. For evaluation of the fission distribution in the NBSR core, a large number of nodes for the fuel plates were used in the MCNPX analysis [3]. Figure 6 shows an elevation view with the axial discretization of the fuel element geometry in the MCNPX model. The plates are modeled without curvature for simplification. The choice of mesh size for the MCNPX calculations is based on the observation that heat conduction in a fuel plate will result in a lateral heat flux profile (i.e. across the width of a fuel plate) that is flatter than the profile of the energy deposition due to fission [11]. The heat conduction problem was analyzed both analytically [11] and numerically [12]. The results indicate the average surface energy flux (sum of energy deposition divided by the surface area of a mesh cell) for a 4 cm^2 mesh conservatively captures the maximum surface heat flux determined by solving the heat conduction problem for a fuel plate. Using this information as guidance for the evaluation of power distribution in the core, the MCNPX calculations employed mesh cells (nodes) with a width of about 2 cm and a height of about 2 cm. There are three cells in the lateral direction and 14 cells in the axial direction per fuel plate. The total number of cells used for the MCNPX analysis is calculated as below.

$$N_{TOT-C} = (\text{Number of cells in lateral direction}) \cdot (\text{Number of cells in axial direction}) \cdot (\text{Number of plates per fuel element}) \cdot (\text{Number of fuel elements})$$

$$N_{TOT-C} = 3 \times 14 \times (2 \times 17) \times 30 = 42{,}840$$

The number of fissions in each cell has been calculated for HEU and LEU fuels at startup (SU), the limiting core condition in terms of the local heat flux and fission rate density, and end-of-cycle (EOC), the limiting core condition in terms of the fission density. It is assumed that all fission energy is deposited directly in the NBSR fuel and within the cell that contains the fission. This assumption is conservative because in reality a small fraction of the fission energy will be deposited directly in the cladding, coolant, moderator, and reactor structural material. Detailed descriptions of the evaluation of power distribution and kinetic parameters by using the MCNPX computer code are presented in [2].

The average fission rate density in the NBSR is calculated based on the core power, the number of nodes in the core, and the volume of each node. The dimensions of each node are 1.9957 cm × 2.04 cm × 0.0215 cm. In the proposed LEU U10Mo fuel the average fission rate density is,

$$Average\,fission\,rate\,density\left|\frac{fission}{cm^3 - s}\right| = (\text{core thermal power}) \times \frac{1}{(\text{fuel volume})}$$

$$= \frac{20 \times 10^6 W}{200 \times 10^6 \text{eV} \times 1.602 \times 10^{-19} \frac{\text{J}}{\text{eV}}} \times \frac{1}{42840 \times 1.9957\,\text{cm} \times 2.04\,\text{cm} \times 0.0215\,\text{cm}} = 1.657 \times 10^{14} \frac{\text{fission}}{\text{cm}^3 - \text{s}}$$

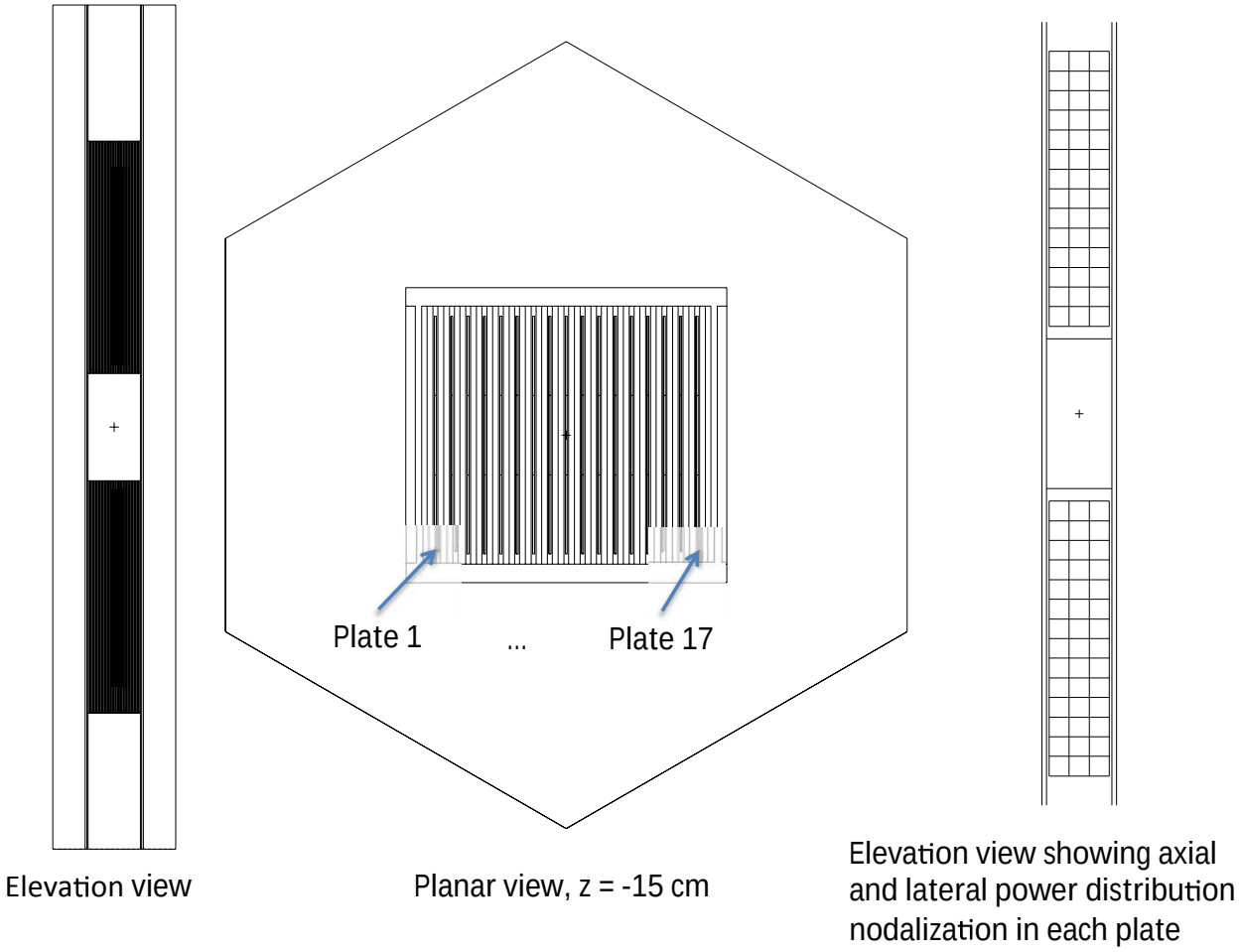

Figure 6 NBSR Fuel Element Geometry in the MCNPX Model

The maximum fission rate density is calculated utilizing the average fission rate density and the node peaking factor. The node peaking factor is the ratio of the peak number of fissions-per-node to the average number of fissions per node, as calculated utilizing the MCNPX model. For the proposed LEU fuel the maximum fission rate density is,

$$Maximum fission rate density \left|\frac{fission}{cm^3 - s}\right|$$
$$= (\text{average fission rate density}) \times (\text{node peaking factor})$$
$$= 1.657 \times 10^{14} \frac{\text{fission}}{\text{cm}^3 - \text{s}} \times 2.431 = 4.029 \times 10^{14} \frac{\text{fission}}{\text{cm}^3 - \text{s}}$$

The limiting core heat flux distribution occurs at SU with fresh shim arms. The core power is more evenly distributed when the shim arms are withdrawn from the core or in a depleted state, because the flux compression in the upper-half of the NBSR core (due to the shim arms) is reduced. This reduces the magnitude of the hot spots and increases the minimum critical heat flux ratio (CHFR). The plate-wise heat flux distributions are plotted in Figure 7 - Figure 10 for the elements with hot spots (maximum number of fissions-per-node) and Figure 11 - Figure 14 for the elements with hot stripes (maximum number of fissions per vertical stripe). Plots are

included for both plate 1 and plate 17. In addition to the limiting cases, the heat flux distributions are also provided for a fresh element, 8-1E, in Figure 15 - Figure 16.

The axial dimension of the fuel element is relative to the axial center of the mid-plane gap (z = 0.0 cm) and the lateral dimension is relative to the lateral center of the fuel plate (y=0.0 cm). The node maximum heat flux of 1394 kW/m^2, corresponding to the maximum fission rate density and a peaking factor of 2.431, occurs on plate 17 of element 8-3E. Element 8-3E is a relatively fresh element, having experienced only two 38.5 day cycles of irradiation. Heat flux distributions are shown for both the inner and outer flow plenum locations. Additionally, the heat flux distributions are shown with fresh shim arms and with shim arms that have been irradiated for twenty-five cycles. The heat flux distribution results for irradiated shim arms are derived from the results of a recent study [10]. The following equation may be utilized to convert a local heat flux to a fission rate density,

$$Fissionratedensity\left[\frac{fission}{cm^3 - s}\right] = q''\left(\frac{kW}{m^2}\right) \times 2.890 \times 10^{11} \frac{fission}{cm^3 - s}\left(\frac{m^2}{kW}\right)$$

		Element 8-7W Lateral position (cm)								
		Plate 1			*Inner plenum*	*Hot spot (SU)*				
		-2.04	0.00	+2.04		-2.04	0.00	+2.04		
Axial position (cm)		**Fresh shim arms**			**Heat flux (kW/m^2)**	**Depleted shim arms**				
36.8		350	371	393	1400	404	424	468		
34.8		394	374	429	1200	428	413	465		
32.8	U	434	410	499	1000	459	435	484		
30.8	p	476	461	513	800	502	467	527		
28.8	p	567	510	547	600	545	502	558		
26.9	e	585	523	595	400	603	550	604		
24.9	r	627	593	655	200	627	592	639		
22.9		672	636	660		682	640	690		
20.9		720	654	722		733	667	722		
18.9		793	731	791		798	725	771		
16.9		861	779	822		850	784	833		
14.9		938	868	919		919	830	904		
12.9		1024	945	1047		1020	939	999		
10.9		1213	1135	1190		1205	1121	1177		
0.0										
-10.9		1376	1286	1315		1290	1220	1281		
-12.9		1189	1067	1128		1156	1059	1143		
-14.9	L	1081	982	1081		1081	972	1040		
-16.9	o	1012	931	1006		1024	926	983		
-18.9	w	997	905	962		981	887	956		
-20.9	e	961	876	929		939	862	934		
-22.9	r	928	830	923		924	829	890		
-24.9		908	824	903		893	820	861		
-26.9		890	797	876		856	805	847		
-28.8		877	805	852		857	774	845		
-30.8		856	805	824		840	771	817		
-32.8		892	785	859		849	776	850		
-34.8		899	815	868		870	783	838		
-36.8		958	906	941		916	866	904		

Figure 7 Heat Flux Distribution, Element 8-7W, Plate 1

		Element 8-7W	***Plate 17***		***Inner plenum***			
	Lateral position (cm)	-2.04	0.00	+2.04		-2.04	0.00	+2.04
Axial position (cm)		**Fresh shim arms**			**Heat flux (kW/m^2)**	**Depleted shim arms**		
36.8		381	384	419	1400	421	425	465
34.8		401	395	425	1200	453	431	493
32.8	U	468	415	481	1000	483	434	497
30.8	p	522	486	517	800	517	483	577
28.8	p	552	497	582	600	565	525	587
26.9	e	600	546	612	400	619	556	617
24.9	r	636	609	661	200	656	602	672
22.9		701	638	704		700	643	698
20.9		751	702	725		765	683	762
18.9		800	712	778		792	718	790
16.9		877	789	854		874	781	851
14.9		954	852	928		951	862	917
12.9		1009	961	1020		1067	959	1029
10.9		1228	1141	1196		1250	1155	1205
0.0								
-10.9		1364	1292	1328		1319	1253	1291
-12.9		1201	1057	1186		1160	1063	1153
-14.9	L	1093	1015	1081		1066	965	1044
-16.9	o	1046	934	1027		1012	907	977
-18.9	w	991	910	985		983	884	943
-20.9	e	961	882	942		960	849	933
-22.9	r	930	863	937		907	819	894
-24.9		930	830	903		902	798	884
-26.9		908	802	855		876	780	851
-28.8		875	791	892		861	767	860
-30.8		892	764	825		850	758	830
-32.8		871	785	834		850	755	837
-34.8		892	814	858		844	787	855
-36.8		952	905	932		908	852	901

Figure 8 Heat Flux Distribution, Element 8-7W, Plate 17

		Element 8-3E					*Plate 1*				*Outer plenum*	*Hot spot (SU)*		
	Lateral position (cm)						-2.04	0.00	+2.04			-2.04	0.00	+2.04
Axial position (cm)							**Fresh shim arms**			**Heat flux (kW/m^2)**		**Depleted shim arms**		
36.8							313	386	487	1400		423	456	538
34.8							306	345	425	1200		399	428	509
32.8	U						332	379	442	1000		411	423	514
30.8	p						404	409	466	800		455	434	506
28.8	p						466	421	521	600		501	469	542
26.9	e						540	459	529	400		545	502	564
24.9	r						603	521	587	200		606	529	583
22.9							644	561	635			654	593	626
20.9							710	606	653			700	611	662
18.9							762	656	729			767	641	718
16.9							820	719	750			821	709	752
14.9							901	766	811			909	782	827
12.9							987	862	903			1008	866	919
10.9							1144	1032	1062			1187	1099	1076
0.0														
-10.9							1394	1194	1216			1348	1189	1199
-12.9							1216	995	1075			1177	1003	1015
-14.9	L						1115	935	952			1091	926	945
-16.9	o						1037	875	923			1039	884	897
-18.9	w						1025	830	903			1010	836	870
-20.9	e						956	830	876			981	820	840
-22.9	r						987	805	857			939	787	844
-24.9							912	829	816			933	768	833
-26.9							928	764	814			908	765	797
-28.8							926	791	796			896	756	763
-30.8							938	742	788			865	743	803
-32.8							891	750	800			906	750	792
-34.8							883	792	854			915	763	795
-36.8							1017	919	935			990	869	909

Figure 9 Heat Flux Distribution, Element 8-3E, Plate 1

		Element 8-3E			***Plate 17***	***Outer plenum***			
		Lateral position (cm)	-2.04	0.00	+2.04		-2.04	0.00	+2.04
Axial position (cm)			**Fresh shim arms**			**Heat flux (kW/m^2)**	**Depleted shim arms**		
36.8			305	364	459	1400	416	464	545
34.8			265	332	427	1200	365	392	505
32.8	U		261	325	432	1000	363	387	504
30.8	p		309	344	465	800	363	387	490
28.8	p		358	368	473	600	432	417	505
26.9	e		411	410	479	400	436	437	526
24.9	r		467	452	551	200	505	468	564
22.9			539	489	577		533	503	583
20.9			583	521	589		599	546	625
18.9			660	585	631		657	587	657
16.9			708	618	664		702	625	681
14.9			785	667	721		780	668	751
12.9			849	745	768		841	751	807
10.9			1040	928	947		1018	915	927
0.0									
-10.9			1178	1043	1047		1158	1053	1034
-12.9			1039	898	923		1025	892	944
-14.9	L		954	845	919		961	819	893
-16.9	o		921	812	858		931	796	859
-18.9	w		895	782	863		910	793	859
-20.9	e		937	749	830		886	769	816
-22.9	r		872	747	824		864	745	822
-24.9			872	746	800		864	743	783
-26.9			861	740	799		820	737	789
-28.8			862	740	841		816	705	780
-30.8			831	737	799		784	730	781
-32.8			850	734	803		837	733	794
-34.8			878	778	828		833	731	823
-36.8			922	868	927		927	839	881

Figure 10 Heat Flux Distribution, Element 8-3E, Plate 17

		Element 8-7E	***Plate***	***1***	***Inner plenum***	***Hot stripe (SU)***		
	Lateral position (cm)	-2.04	0.00	+2.04		-2.04	0.00	+2.04
Axial position (cm)		**Fresh shim arms**			**Heat flux (kW/m^2)**	**Depleted shim arms**		
36.8		388	375	366	1400	427	417	423
34.8		426	379	418	1200	463	409	444
32.8	U	466	440	450	1000	489	441	494
30.8	p	500	465	522	800	539	461	521
28.8	p	533	521	532	600	560	511	571
26.9	e	612	548	587	400	591	557	611
24.9	r	640	612	665	200	655	597	647
22.9		672	621	705		694	644	703
20.9		728	676	734		758	667	732
18.9		820	734	777		802	714	790
16.9		877	770	840		865	768	836
14.9		972	861	922		937	849	910
12.9		1037	934	1039		1034	947	1023
10.9		1247	1138	1174		1213	1148	1169
0.0								
-10.9		1345	1255	1339		1301	1229	1284
-12.9		1186	1093	1175		1174	1061	1149
-14.9	L	1125	1016	1078		1092	941	1054
-16.9	o	1032	946	1013		1019	916	989
-18.9	w	978	896	979		971	847	943
-20.9	e	955	873	960		927	844	926
-22.9	r	934	837	911		936	827	915
-24.9		958	832	913		890	812	870
-26.9		891	794	896		880	805	850
-28.8		916	839	854		862	787	856
-30.8		875	799	847		874	756	825
-32.8		888	785	857		863	754	828
-34.8		895	832	897		873	804	860
-36.8		947	918	918		933	864	909

Figure 11 Heat Flux Distribution, Element 8-7E, Plate 1

Element 8-7E ***Plate 17*** ***Inner plenum***

Axial position (cm)		Fresh shim arms Lateral position (cm) -2.04	0.00	+2.04	Heat flux (kW/m^2)	Depleted shim arms -2.04	0.00	+2.04
36.8		387	354	330	1400	420	387	398
34.8		403	357	347	1200	432	378	418
32.8	U	428	394	406	1000	472	419	444
30.8	p	485	453	486	800	499	443	492
28.8	p	523	494	535	600	556	487	533
26.9	e	589	534	572	400	582	540	576
24.9	r	641	568	606	200	648	591	619
22.9		661	605	667		670	628	688
20.9		751	641	731		725	670	715
18.9		775	713	786		775	709	784
16.9		862	789	824		836	771	833
14.9		909	825	914		914	834	885
12.9		1048	905	1028		1011	934	980
10.9		1183	1104	1176		1199	1111	1182
0.0								
-10.9		1355	1277	1321		1332	1242	1295
-12.9		1187	1102	1164		1149	1069	1149
-14.9	L	1074	977	1075		1051	966	1055
-16.9	o	1033	940	1036		1019	930	1012
-18.9	w	985	899	1019		985	874	935
-20.9	e	960	876	957		928	839	925
-22.9	r	945	812	910		931	820	885
-24.9		920	828	896		894	830	880
-26.9		896	822	887		875	795	862
-28.8		851	795	863		839	759	824
-30.8		875	807	836		832	760	809
-32.8		872	781	834		856	768	813
-34.8		878	799	847		841	789	832
-36.8		944	875	948		927	862	900

Figure 12 Heat Flux Distribution, Element 8-7E, Plate 17

		Element 7-2E	*Plate 1*			*Outer plenum*		*Hot stripe (SU)*	
	Lateral position (cm)	-2.04	0.00	+2.04			-2.04	0.00	+2.04
Axial position (cm)		**Fresh shim arms**			**Heat flux (kW/m^2)**		**Depleted shim arms**		
36.8		781	703	779	1400		816	740	790
34.8		736	614	688	1200		763	668	727
32.8	U	738	615	682	1000		741	663	701
30.8	p	739	628	683	800		745	648	711
28.8	p	727	649	700	600		780	639	715
26.9	e	765	643	679	400		780	659	724
24.9	r	798	670	707	200		806	695	724
22.9		791	689	732			830	696	765
20.9		870	733	807			855	741	762
18.9		889	724	817			887	754	814
16.9		950	764	845			937	794	831
14.9		1021	842	881			1001	833	881
12.9		1074	916	955			1104	933	970
10.9		1311	1145	1145			1310	1127	1131
0.0									
-10.9		1363	1197	1183			1351	1136	1185
-12.9		1181	996	1041			1160	993	984
-14.9	L	1110	881	912			1058	901	911
-16.9	o	1029	867	890			1024	830	890
-18.9	w	1005	811	870			992	821	849
-20.9	e	985	783	829			946	769	787
-22.9	r	947	762	807			905	754	763
-24.9		920	752	765			903	739	739
-26.9		901	715	740			862	714	753
-28.8		853	708	736			858	709	724
-30.8		866	706	740			848	694	697
-32.8		858	675	737			853	696	713
-34.8		849	726	736			857	694	718
-36.8		957	809	808			930	791	790

Figure 13 Heat Flux Distribution, Element 7-2E, Plate 1

		Element 7-2E			***Plate 17***	***Outer plenum***			
		Lateral position (cm)	-2.04	0.00	+2.04		-2.04	0.00	+2.04
Axial position (cm)			**Fresh shim arms**			**Heat flux (kW/m^2)**	**Depleted shim arms**		
36.8			741	683	734	1400	781	719	789
34.8			661	593	661	1200	698	632	701
32.8	U		645	557	658	1000	676	615	693
30.8	p		651	587	639	800	668	600	671
28.8	p		648	594	645	600	697	616	693
26.9	e		679	589	671	400	717	607	694
24.9	r		688	572	671	200	738	646	716
22.9			729	618	736		735	654	705
20.9			795	654	713		774	672	757
18.9			830	690	750		826	701	773
16.9			866	693	782		872	739	803
14.9			929	800	839		933	788	851
12.9			1007	849	925		1020	898	950
10.9			1204	1058	1110		1230	1070	1098
0.0									
-10.9			1269	1116	1168		1284	1120	1134
-12.9			1114	952	968		1098	929	983
-14.9	L		1018	839	917		1020	832	902
-16.9	o		931	796	844		942	794	848
-18.9	w		906	740	821		888	760	809
-20.9	e		851	728	778		870	710	789
-22.9	r		881	694	747		846	706	748
-24.9			856	683	766		842	678	729
-26.9			828	677	749		798	661	728
-28.8			786	659	716		804	646	685
-30.8			766	626	702		760	643	678
-32.8			775	646	688		781	628	665
-34.8			811	672	708		783	657	672
-36.8			883	805	778		882	767	769

Figure 14 Heat Flux Distribution, Element 7-2E, Plate 17

		Element 8-1E					*Plate 1*			*Outer plenum*	*Fresh Element*		
		Lateral position (cm)					-2.04	0.00	+2.04		-2.04	0.00	+2.04
Axial position (cm)							**Fresh shim arms**			**Heat flux (kW/m^2)**	**Depleted shim arms**		
36.8							701	651	752	1400	745	737	781
34.8							632	591	669	1200	674	606	708
32.8	U						620	566	634	1000	642	605	658
30.8	p						587	587	656	800	644	595	676
28.8	p						595	571	663	600	663	585	701
26.9	e						665	594	653	400	687	593	713
24.9	r						664	624	702	200	694	619	682
22.9							713	633	699		710	654	722
20.9							735	664	747		732	664	752
18.9							759	716	769		771	678	755
16.9							834	705	793		801	746	802
14.9							886	762	806		886	782	830
12.9							927	873	916		970	843	910
10.9							1135	1011	1038		1149	1048	1063
0.0													
-10.9							1195	1067	1098		1191	1085	1097
-12.9							1049	908	957		1016	904	947
-14.9	L						975	862	882		930	820	885
-16.9	o						896	770	837		887	751	822
-18.9	w						856	736	804		844	758	812
-20.9	e						851	743	824		832	733	808
-22.9	r						834	723	797		817	682	761
-24.9							818	696	748		790	695	739
-26.9							775	669	761		780	668	729
-28.8							769	649	706		771	650	711
-30.8							763	672	721		742	633	696
-32.8							737	649	693		771	630	664
-34.8							798	670	703		758	662	694
-36.8							885	765	801		874	761	773

Figure 15 Heat Flux Distribution, Element 8-1E, Plate 1

		Element 8-1E	*Plate 17*			*Outer plenum*			*Fresh Element*
	Lateral position (cm)	-2.04	0.00	+2.04		-2.04	0.00	+2.04	
Axial position (cm)		**Fresh shim arms**			**Heat flux (kW/m^2)**	**Depleted shim arms**			
36.8		680	656	725	1400	737	687	744	
34.8		613	557	663	1200	637	633	678	
32.8	U	570	541	604	1000	644	584	657	
30.8	p	585	543	643	800	644	575	672	
28.8	p	609	571	625	600	643	585	666	
26.9	e	631	584	665	400	656	595	687	
24.9	r	628	610	655	200	663	603	675	
22.9		666	593	684		701	620	691	
20.9		713	627	714		698	624	725	
18.9		726	627	755		725	645	756	
16.9		760	644	768		760	668	748	
14.9		801	676	784		815	727	790	
12.9		874	768	820		874	766	855	
10.9		1030	892	963		1010	925	959	
0.0									
-10.9		1092	956	985		1079	961	994	
-12.9		949	814	858		950	819	894	
-14.9	L	881	760	827		888	747	809	
-16.9	o	866	759	820		845	748	778	
-18.9	w	851	701	789		831	713	790	
-20.9	e	816	728	771		801	693	772	
-22.9	r	822	722	750		786	679	754	
-24.9		781	694	739		774	682	738	
-26.9		775	670	731		758	652	725	
-28.8		804	671	724		753	646	684	
-30.8		744	638	700		758	648	699	
-32.8		766	645	701		771	630	684	
-34.8		772	660	704		777	666	689	
-36.8		869	782	768		857	761	759	

Figure 16 Heat Flux Distribution, Element 8-1E, Plate 17

4. High-Resolution LEU Power Distribution for Element 8-3E

This section documents the calculation of high resolution power peaking in the LEU fuel element with the maximum fission rate density. The calculation was performed utilizing a fine mesh tally (TMESH) in MCNPX. The objective was to be able to inform the design of the irradiation experiment by offering a snapshot of the expected power distribution on a fine mesh. The lower half of fuel element 8-3E experiences the peak fission rate density in the LEU NBSR and was thus selected as a case study.

Mesh tallies were used to examine the energy deposition within the selected plates from element 8-3E. The mesh interval dimensions for the upper and lower plates were $<i = 1, j = 30, k = 50>$. The *i*-nodes correspond to the x-direction (lateral), *j*-nodes correspond to the y-direction (transverse), and *k*-nodes correspond to the z-direction (height). This yields 30 mesh points in the transverse direction, which constitutes a resolution less than 0.1 inch. This energy deposition distribution assumes uniform burn-up within the fuel element. The x-coordinate defines the location of the relevant plate.

Six locations were selected for analysis, two in the lower half of plate 1, two in the lower half of plate 9, one in the upper half of plate 1, and one in the upper half of plate 9. The results for plate 9 were included because the inner plates (plate 2 – plate 16) feature significant gradients in the relative power distributions when compared to the outer plates (plate 1 and plate 17). The local relative power peaking (normalized to unity) was plotted at each selected axial location. This normalization shows the local transverse variation. The results are shown in Figure 17 - Figure 19 for plate 1 and Figure 20 - Figure 22 for plate 9. The selected axial locations for the plots are shown in Figure 23; these location designators are superimposed upon a contour plot of the power density in the lower and upper halves of plate 1. The units in this contour plot are relative, with blue tones representing the lowest power densities in the plate and red tones representing the highest power densities in the plate. A higher resolution view of the power density distribution in the bottom half of plate 1 is shown in Figure 24. This contour plot has been rotated 90 degrees clockwise.

Mesh points that contain partial volume fractions of fuel meat and cladding are removed from the transverse extremities of the plots. The error bars are derived from the relative uncertainty in each mesh element. The relative uncertainty of the tallies within the fuel material is usually below 5%. The error propagation makes the assumption that the uncertainties in the mesh tallies are independent and random. Quadratic fits are added to the plots to emphasize the average behavior of the tallies. Emphasis was placed on the transverse direction, because sufficient axial resolution is detailed in the previous section.

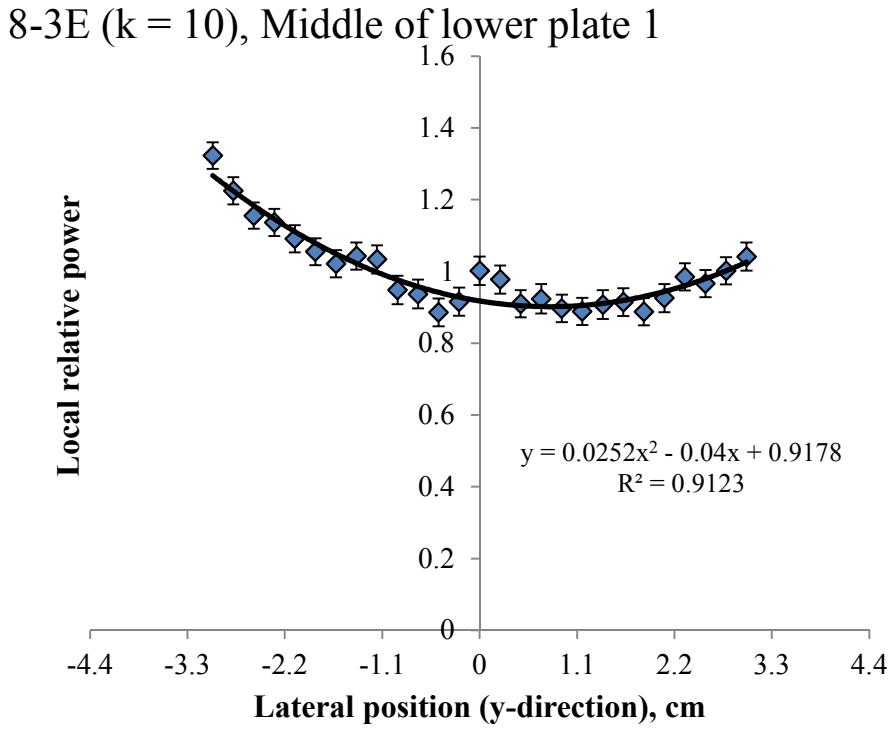

Figure 17 Transverse Power Profile for Element 8-3E, Plate 1, at Axial Node <k=10>

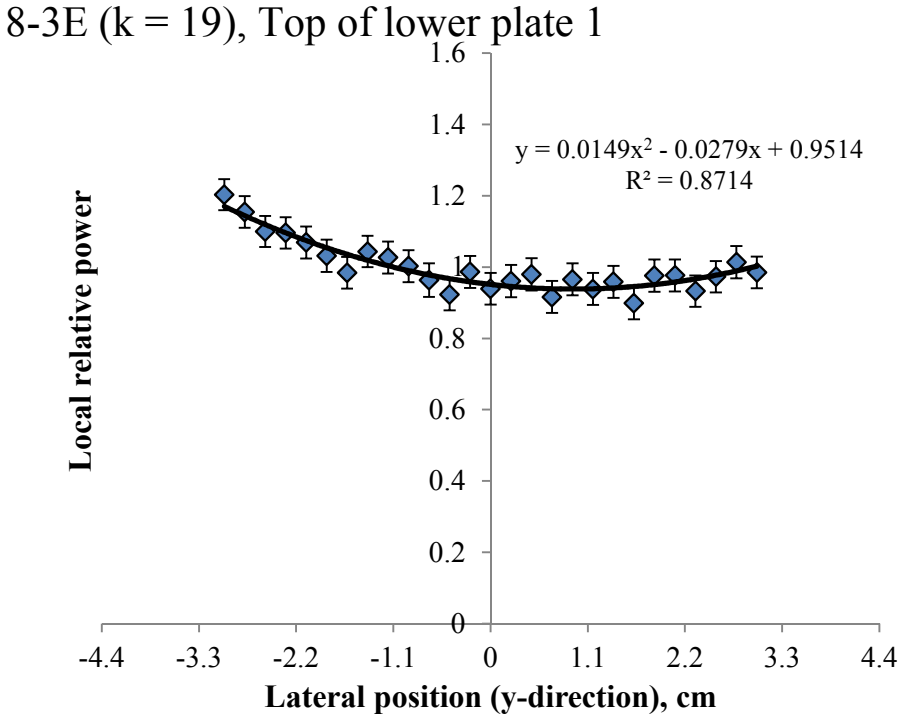

Figure 18 Transverse Power Profile for Element 8-3E, Plate 1, at Axial Node <k=19>

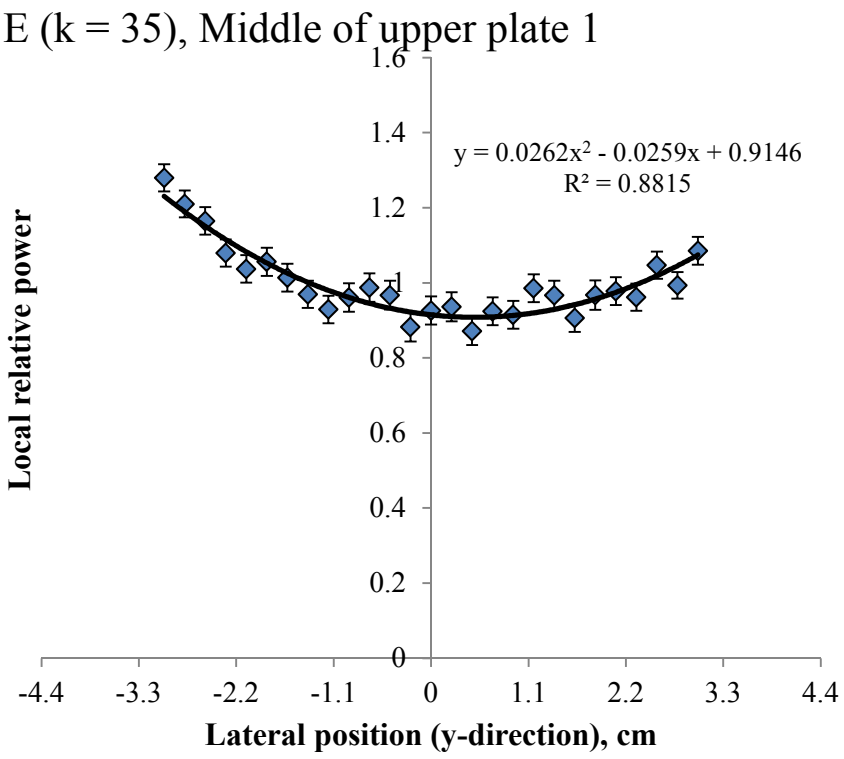

Figure 19 Transverse Power Profile for Element 8-3E, Plate 1, at Axial Node <k=35>

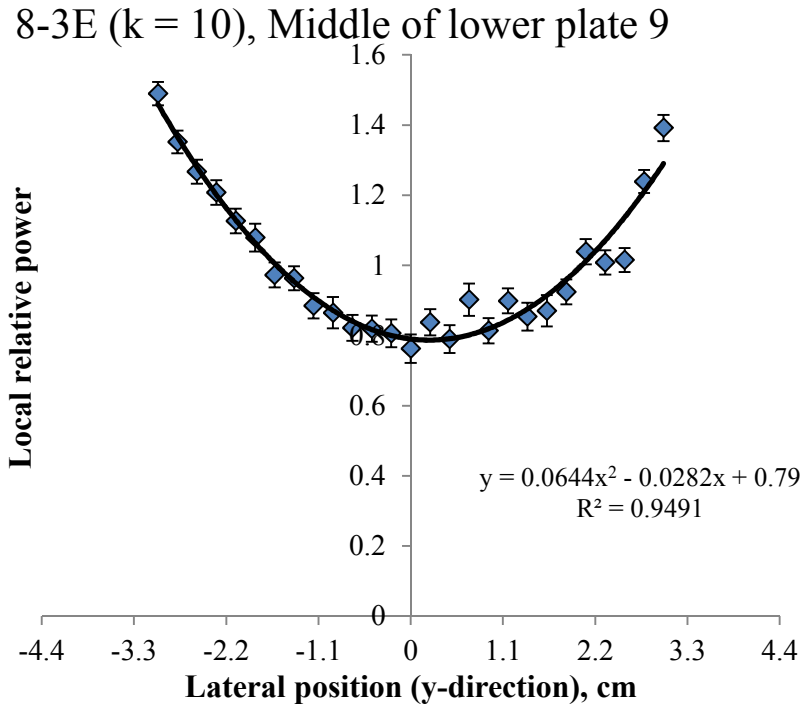

Figure 20 Transverse Power Profile for Element 8-3E, Plate 9, at Axial Node <k=10>

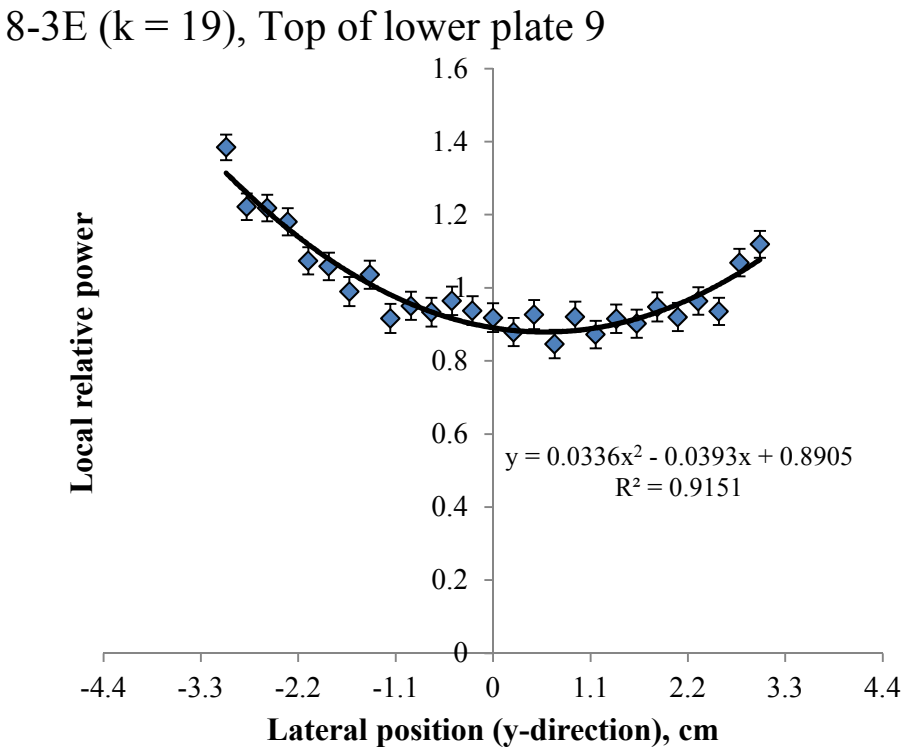

Figure 21 Transverse Power Profile for Element 8-3E, Plate 9, at Axial Node <k=19>

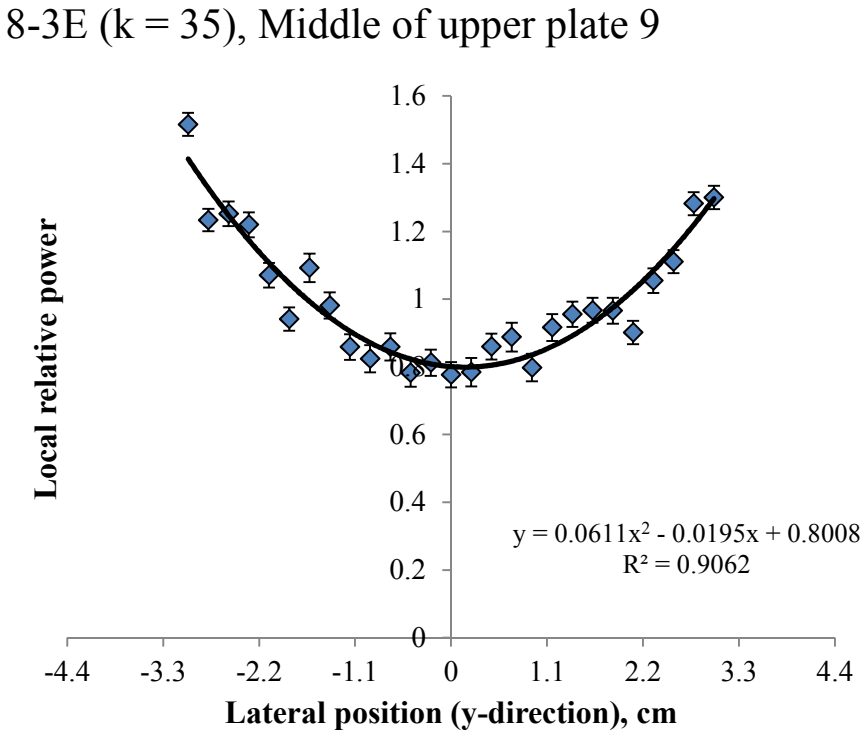

Figure 22 Transverse Power Profile for Element 8-3E, Plate 9, at Axial Node <k=35>

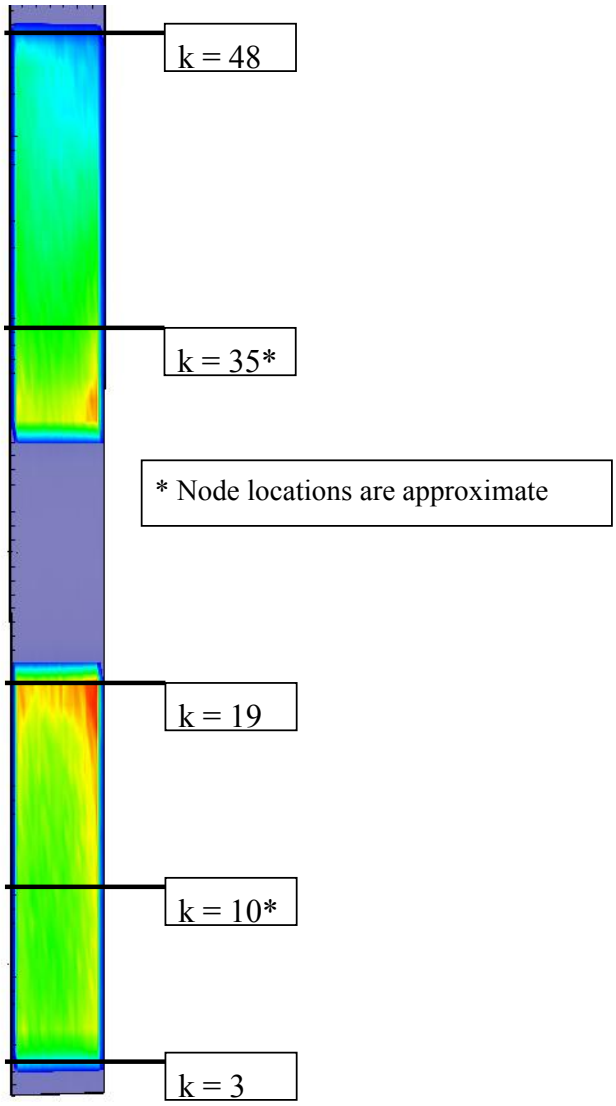

Figure 23 Selected Axial Locations for the Transverse Power Profiles for 8-3E, Plate 1

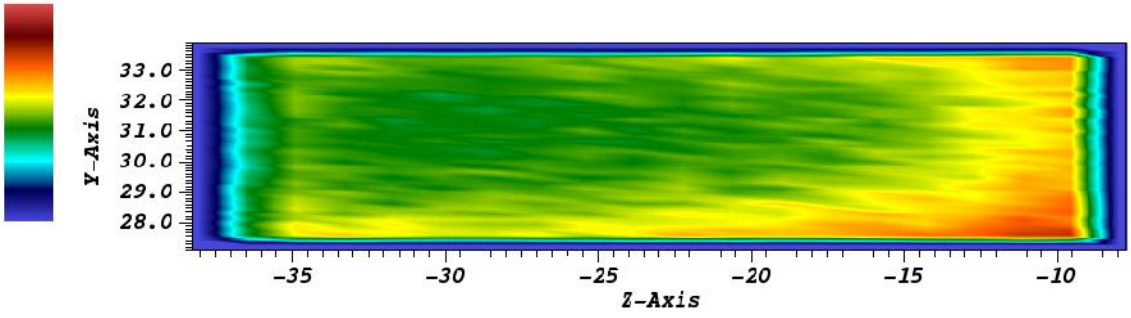

Figure 24 2-D Power Distribution for 8-3E, in the Bottom Half of Plate 1 (Relative Units, Rotated +90 degrees)

5. Limiting LEU Local Burn-Up and Fission Density

The purpose of this section is to inform the design and planning of future irradiation experiments by documenting the calculated cumulative fission density in the LEU NBSR. The calculation of the average cumulative fission density depends on the average fission rate density and the average core residence time (7.5 cycles of 38.5 days),

$$Average fission density \left|\frac{fission}{cm^3}\right|$$
$$= (\text{average fission rate density}) \times (\text{core residence time})$$
$$= 1.657 \times 10^{14} \frac{\text{fission}}{\text{cm}^3 - \text{s}} \times 7.5 \times 38.5\,\text{day} \times \frac{86400\,\text{s}}{\text{day}} = 4.134 \times 10^{21} \frac{\text{fission}}{\text{cm}^3}$$

To obtain the maximum fission density (local burn-up) is more complex. In the equilibrium LEU core model the fuel inventories are homogenized within each half-element. However, recent studies have investigated the distribution of burn-up within the NBSR half-element [5]. These studies have shown two effects: (1) the impact of the mid-plane gap on axial burn-up and (2) the impact of the plate-to-plate self-shielding on the plate-wise burn-up. The impact of these two effects was not considered synergistically. The study was accomplished via a single element model without shim arms. Thus, the impact of the shim arms, which will increase the local fission density in the lower half-element and decrease the local fission density in the upper half-element, is also not reflected in these results.

An estimate of the maximum fission density is based on the full core model utilized for the development of the equilibrium LEU core design [2]. The approach utilizes the full-core model to tally the local flux distribution in the top nodes of the bottom half-element that experiences the peak local fission rate density in the NBSR. The cell tallied is the top axial node (out of the 14 axial nodes) that spans all 17 plates and three transverse nodes for each plate. To account for the plate-wise and transverse power peaking, multipliers are used for the flux normalization factor in the following depletion calculation.

These 63-group flux tallies are utilized as a boundary condition for a depletion analysis using the stand-alone CINDER'90 tool [13]. The flux tallies for each cycle come from a single static calculation for the start-up core, when the flux compression in the top of the bottom fuel elements is most severe. The flux was not re-calculated with new inventories; inventories were based on the original half-element depletion. Because of this, it is expected that the results will be bounding since the fluxes tallied are based on calculations where local fission rates at the top node in later cycles are over-predicted by up to 50% [5]. CINDER'90 integrated within MCNPX is the depletion tool utilized in the equilibrium core calculation. Within CINDER'90, the fuel compositions are depleted for 38.5 days using a depletion time-step of approximately two days, with each cycle followed by 10.5 days of decay. The cycle-by-cycle flux tallies provide the neutron sources for the depletion calculations. These flux tallies are shown in Figure 25.

The results for the fission density based on the cycle-by-cycle depletion calculation are shown in Figure 26. A solid line intercepting the y-axis of the plot indicates the bounding fission density at the end of cycle 8, 7.16E+21 fissions/cc. A dashed line intercepting the y-axis indicates the bounding fission density at the end of a hypothetical cycle 9, 7.61E+21 fissions/cc. The value

for cycle 9 is based on an additional cycle of operation following cycle 8, with the cycle 8 flux tally utilized as the neutron source. In Fall 2013, the NBSR had an event where they operated using three fresh fuel elements instead of four and maintained an end-of-life (cycle-7) fuel element in the core for an additional cycle. Thus the average fuel residence time in the core was extended when compared to nominal conditions. The cycle 9 value is intended to credibly bound hypothetical future fuel perturbation scenarios involving 8-cycle fuel elements.

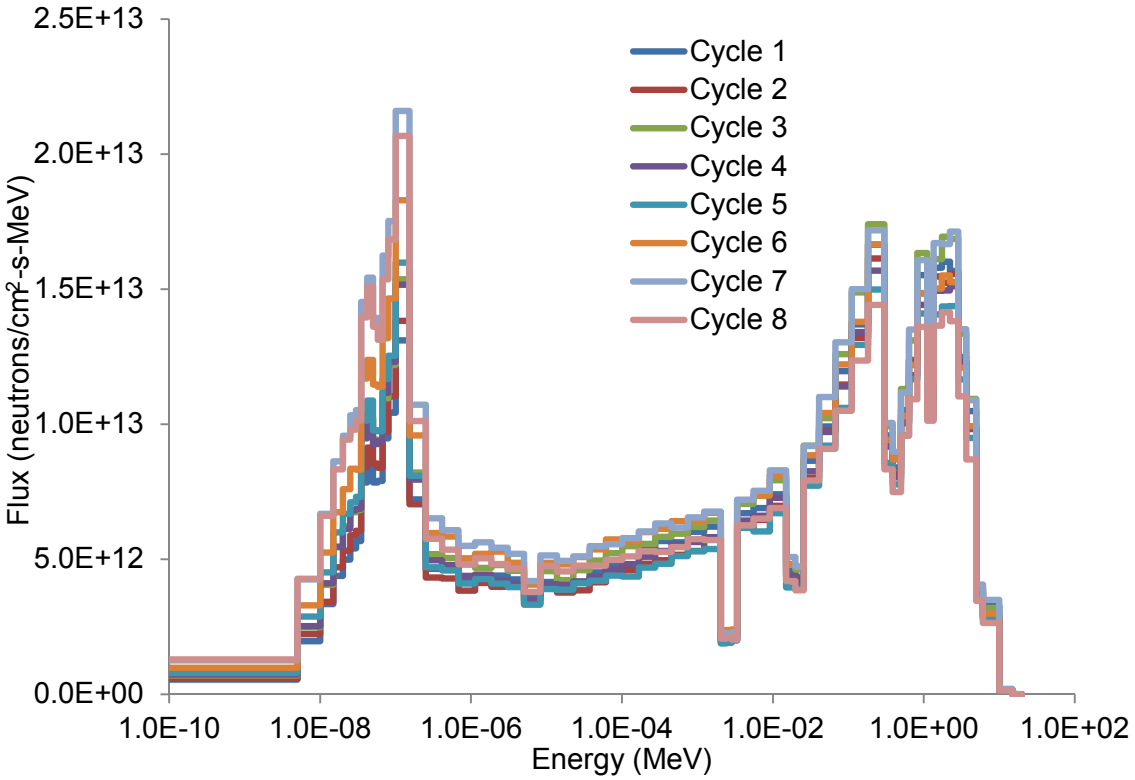

Figure 25 Flux Tallies in the Fuel Meat Utilized in the Depletion Calculation

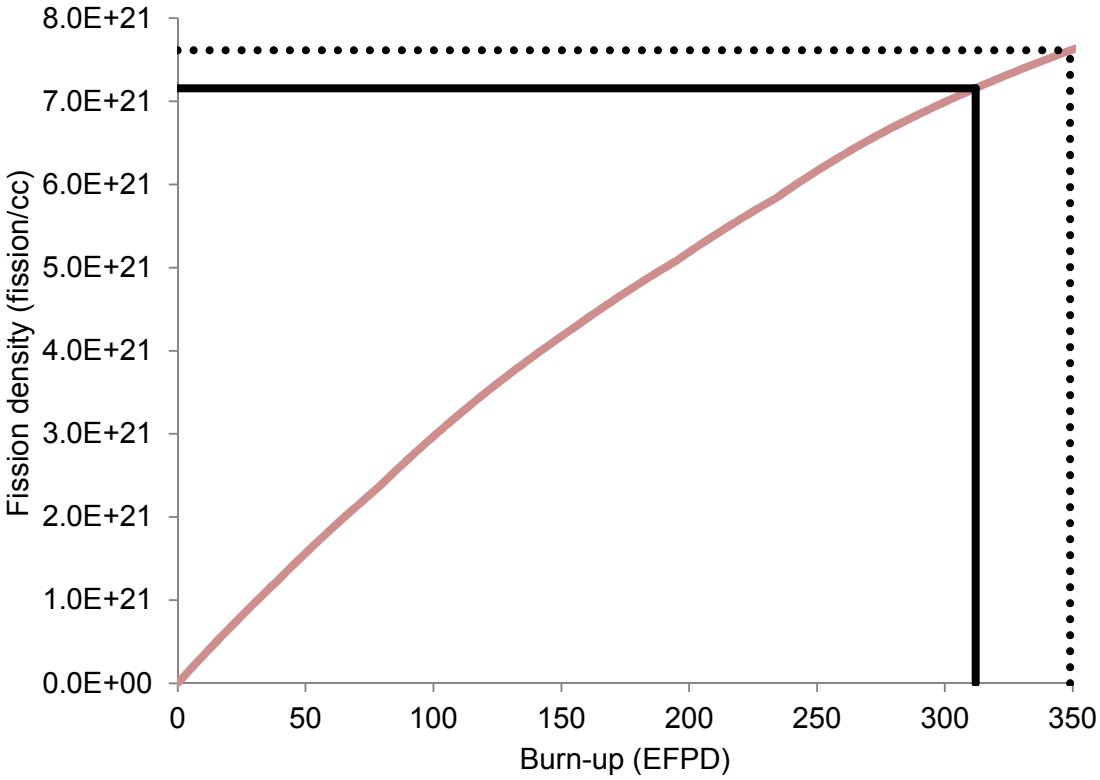

Figure 26 Recommended Peak Fission Density in the LEU NBSR

6. Limiting Fuel Temperatures

The thermal-hydraulic safety analysis for the NBSR has been documented in Reference [8]. The tool utilized for the safety analysis is RELAP5. As described in Reference [3], the power distributions in the RELAP5 model are derived from the full-core power distributions calculated using MCNPX. The channels with hot spots and hot stripes are modeled using a conservative methodology to simplify the power distributions calculated with MCNPX. Nuclear hot channel factors (for example, local power peaking) are modeled but engineering hot channel factors (for example, uncertainties in fuel meat thickness) are not explicitly considered in this analysis. A summary of some relevant assumptions is included here, but full discussion may be found elsewhere [3].

In the RELAP5 model, five flow channels are used to model the six inner plenum fuel elements and eight flow channels are used to represent the twenty-four outer plenum fuel elements. It is assumed in the NBSR model that the core channel flow paths are connected in parallel and the power to each channel is determined based on the fission distribution calculated by MCNPX. Each core channel has heat structures representing the fuel plates in the lower and upper core regions. A core channel may represent multiple fuel plates lumped together as an effective plate with an effective flow channel representing the flow through the plated and un-plated regions. The RELAP5 analysis only accounts for one-dimensional heat transfer from the fuel to the

coolant and no axial or lateral heat conduction in the fuel plate is modeled. A hydraulic flow channel is shown in Figure 27.

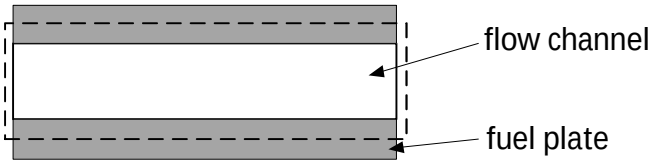

Figure 27 Hydraulic Flow Channel (shown horizontally)

The heat generated in a fuel plate is transferred to the two adjacent flow channels. In the analysis it is assumed that the power generated in the hottest plate is transferred into one common flow channel as shown in the lower diagram in Figure 28. This is conservative for two reasons. Firstly, the hottest plate, by definition, is next to a plate that is not as hot (plate A in Figure 28) and secondly, it is observed from the power distribution analysis that the hottest plate is always the outer-most plate in a fuel element. The latter means that one side of the hottest plate faces a channel that has an unfueled aluminum plate on the other side (plate B in Figure 28) and hence, has cooler water on that side. The heat flux into this cooler outside channel q''_B is more than the average heat flux from the hottest plate and the heat flux into the hot channel q''_A will actually be less than the average heat flux (q'') from that plate.

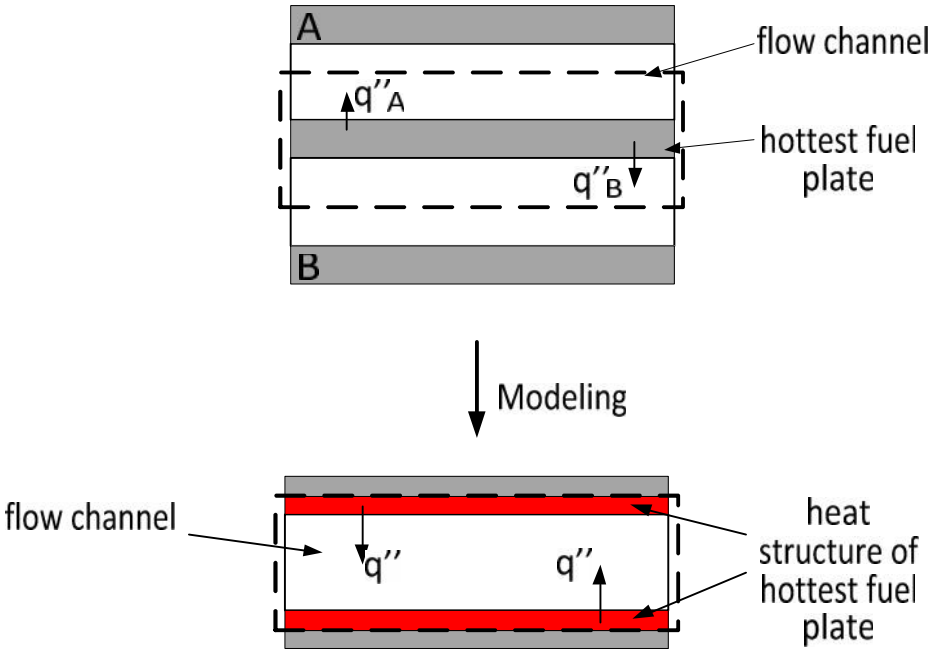

Figure 28 Heat Transfer Modeling Simplifications in a Flow Channel

The power distribution in the NBSR core is modeled using heat structures for flow channels. A FORTRAN program has been developed to read the very detailed fission information in each cell, as calculated by MCNPX. The program examines the hottest cells where the highest power is produced in the inner and outer core plenum.

The power distributions are examined along the axial cells that include the hottest cell. This is called a "fuel stripe" and represents one-third of a fuel plate. This is illustrated in Figure 29. The model is conservatively simplified by assuming that the power distribution in the hottest axial stripe is the same in the remaining two lateral stripes. This methodology is illustrated in Figure 29.

The steady state axial fuel meat centerline temperature distribution is shown in Figure 30 for the most limiting LEU core condition. Even though the methodology for obtaining the power distribution in RELAP5 is conservative, the predicted fuel meat temperatures are less than 390 K for all nodes.

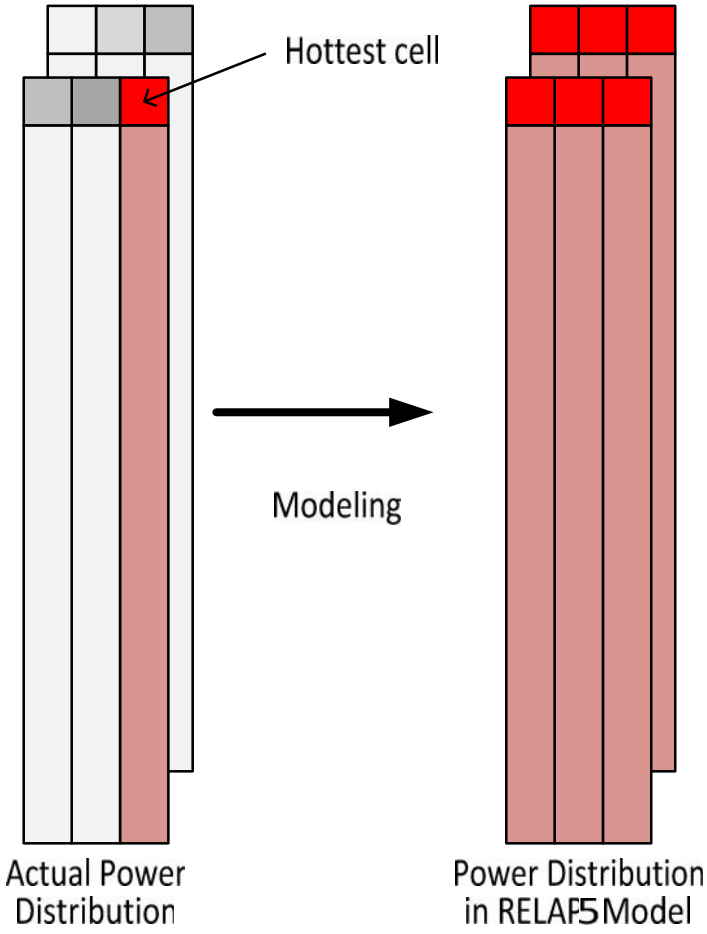

Figure 29 Modeling of Power Distribution in the RELAP5 Input Model

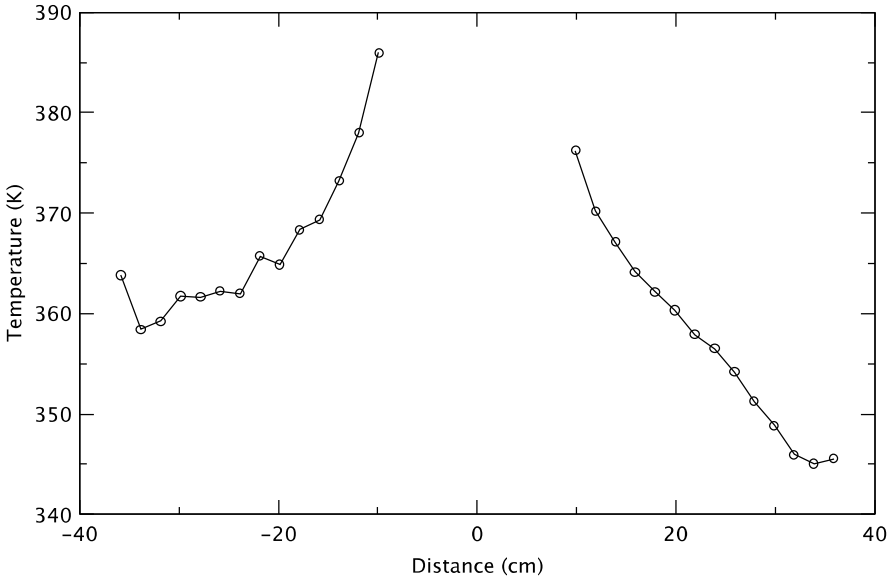

Figure 30 Axial LEU Fuel Meat Centerline Temperature Distribution (Limiting Core Condition)

7. Tolerance Assumptions and Hot Channel Factors in the Safety Analyses

This section provides the reactor fuel parameters, and tolerances or uncertainties, utilized in the safety analyses. This includes the uncertainties utilized to provide cumulative distribution functions for critical heat flux ratio (CHFR) and onset of flow instability ratio (OFIR), the limiting thermal hydraulic quantities used in the safety analysis. Details of this statistical analysis are given in Reference [15]. Hot channel factors are also applied to some of the key requested metrics.

Table 2 shows the geometry and material assumptions utilized in the safety analysis (SA) for both the HEU and the LEU cores. The source of the information is also given. Tolerances in the table are limiting values. Table 3 shows the hot channel factors (HCFs or standard deviations) utilized in the statistical hot channel analysis. Tolerances or uncertainties in geometric quantities for LEU fuel can be assumed to be the same as for the HEU fuel. For material quantities, for example, local fuel loading, the tolerance is expected to be as good as for HEU. However, these are subjective evaluations and may be modified when more is known about fuel fabrication. Table 4 shows the peak local values of fission rate, fission density, and heat flux for the LEU core under nominal conditions and using the current estimates for hot channel factors and assuming they can be combined statistically (using root mean square).

Table 2 Geometry and Material Assumptions

Parameter	HEU Specification	LEU Analysis Assumes
Maximum channel width (at plate center)	116 ± 7 mil [16]	116.0 ± 7 mil (same as HEU)
Average channel width	114 mil [8]	114 mil [8]
Minimum channel width for SA	107.5 mil [8]	107.5 mil [8]
Plate thickness	50 mil [16]	50 mil [2]
Clad thickness	15 mil [16]	20.8 mil [2] (including 1.0 ± 0.5 mil Zr layer [17])
Minimum clad thickness	10.5 mil, not used in SA [16]	10.5 mil, not used in SA [18]
Clad scratch maximum depth	< 5 mil (over fuel meat), not used in SA	< 5 mil (over fuel meat), not used in SA [18]
Clad dent maximum depth	<6 mil, not used in SA	<6 mil, not used in SA [18]
Fuel meat	U_3O_8 dispersion in Al	U10Mo alloy with Mo 10 ± 1 w/o [17]
Fuel meat thickness	20 mil	8.5 ± 1 mil [2]
U-235 enrichment	93 ± 1 w/o [16]	19.75 ± 0.20 w/o [17]
Average U-235 fuel loading (plate)	10.294 ± 0.2 g [16]	11.265 ± 0.24 g, based on Mo and enrichment uncertainties [17]
Bonding integrity	Fuel is subjected to blister test at 482 ± 11°C for at least one hour.	Debond characterization and tolerances TBD
Local fuel homo-geneity	112% of nominal [16]	112% of nominal
Fission density limit	<3.1E21 fission/cc (100% U-235 burnup)	7.2E21 fission/cc [7]
U-10Mo specific heat; U10Mo thermal conductivity	Not applicable (NA)	Values provided in [19] and [20]. Uncertainties are not available or used in the safety analysis.

Table 3 Hot Channel Factors and References to Underlying Tolerances [15]

Source of Uncertainty	HEU Limit*	HEU Reference	LEU Limit*	LEU Reference
Reactor power measurement**	0.025	Table 3.2-1 in [21]	0.025	NBSR data
Power density calculation	0.04	Table 3.2-1 in [21]	0.04	Engineering judgment [15]
Channel dimensional tolerance (local)	0.042	Dwg # E-04-016 in [16]	0.042	Same as HEU
Channel dimensional tolerance (average)	0.035	Dwg # E-04-016, in [16]	0.035	Same as HEU
Velocity distribution measurement**	0.025	Sect. 4.7.4.5, 4.7.4.6 in [22]	0.025	NBSR data
Primary flow rate measurement**	0.006	[23]	0.006	NBSR data
Fuel loading tolerance (local)	0.069	NBSR fuel specification [16]	0.069	Same as HEU [15]
Fuel loading tolerance (average)	0.0112	NBSR fuel specification [16]	0.0123	Based on Mo and enrichment uncertainties [17]
Heat transfer correlation	0.087	Engineering judgment, not used	0.087	Same as HEU
Critical heat flux correlation	0.202	Sudo-Kaminaga correlation [24]	0.202	Same as HEU
OFI heat flux correlation	0.153	Saha-Zuber correlation [25]	0.153	Same as HEU

* Uncertainty limits represent 1 σ standard deviation assuming a normal distribution. When the referenced uncertainties were given as lower and upper limits, the range is assumed to represent a $\sqrt{12}$ σ value.

** Measurement uncertainties based on data from NBSR.

Table 4 Peak Steady State Values

Core Condition	**Fission Rate Density** (fissions/cm^3-s)	**Fission Density** (fissions/cm^3)	**Heat Flux** (kW/m^2)
Maximum Licensed Power without HCFs (20 MW)	4.03E+14	7.16E+21	1394
Hot Channel Factors			
^{235}U Homogeneity (Peak)	1.069	1.069	1.069
Calculated Power Distribution	1.040	-	1.040
Power Measurement	1.025	-	1.025
Total	1.048	1.069	1.048
Maximum Licensed Power with HCFs (20 MW)	4.22E+14	7.65E+21	1461
LSSS Power (26 MW) with HCFs	5.24E+14	NA	1812

8. Summary

This report presents a compilation of requested information relevant to the design of irradiation experiments for the LEU NBSR fuel. This report is intended to provide only the significant highlights of the LEU NBSR core design and safety analysis. An effort has been made to present best-estimate results for the most limiting LEU core conditions. The channels with hot spots and hot stripes were modeled with a methodology for simplifying the core power distributions that produces conservative results. Additional detail regarding the methods utilized in the calculations is provided in the relevant references, although the context and presentation differs from this document. A summary of some of the requested metrics is presented in Table 5.

Table 5 Values of the Requested Metrics

Parameter	Value
Average fission rate density (10^{14} fission/cm^3-s)	1.657
Peak fission rate density (10^{14} fission/cm^3-s)	4.029
Average heat flux (kW/m^2)	573
Peak heat flux (kW/m^2)	1394
Average fission density (10^{21} fission/cm^3)	4.134
Peak fission density (10^{21} fission/cm^3)	7.16
Fuel meat temperature (K)	< 390

9. References

[1] NIST, "Safety Analysis Report (SAR) for License Renewal for the National Institute of Standards and Technology Reactor - NBSR; NBSR-14, Rev. 4," U.S. Department of Commerce, NISTIR 7102, National Institute of Standards and Technology, 2010. Note that this is a modified version of the original NBSR-14 issued in 2004.

[2] A. L. Hanson and D. J. Diamond, "Calculation of Design Parameters for an Equilibrium LEU Core in the NBSR," BNL Technical Report, Brookhaven National Laboratory, September 29, 2011.

[3] J-S. Baek, "Power Distribution in NBSR Core for RELAP5 Safety Analysis," BNL Technical Report, Brookhaven National Laboratory, May 25, 2012.

[4] A. L. Hanson, N. R. Brown, and D. J. Diamond, "Effect of Shim Arm Depletion in the NBSR," BNL Technical Report (BNL-99764-2013-IR), Brookhaven National Laboratory, February 21, 2013.

[5] N. R. Brown, A. L. Hanson, and D. J. Diamond, "Local Burn-Up Effects in the NBSR Fuel Element," BNL Technical Report (BNL-99145-2013-IR), Brookhaven National Laboratory, January 23, 2013.

[6] A. L. Hanson, "The Maximum Burnup in an NBSR Fuel Element," BNL Memorandum, Brookhaven National Laboratory, February 9, 2012.

[7] N. R. Brown, A. L. Hanson, and D. J. Diamond, "Revised Estimates for the Maximum Fission Density in the NBSR," BNL Memoorandum, Brookhaven National Laboratory, February 21, 2014.

[8] J-S. Baek, A. Cuadra, A. L. Hanson, L-Y. Cheng, N. R. Brown, and D.J. Diamond, "Accident Analysis for the NIST Research Reactor Before and After Fuel Conversion – Revision 1," BNL Technical Report (BNL-98524-2012-IR-R1), Brookhaven National Laboratory, June 25, 2013`.

[9] E. H. Wilson, “Irradiation Conceptual Design Parameters,” Electronic mail communication, Argonne National Laboratory, February 4, 2013.

[10] D.B. Pelowitz, "MCNPX Users Manual Version 2.7.0," LA-CP-11-00438, Los Alamos National Laboratory, 2011.

[11] J. M. Rowe, “Choice of Mesh Size for Hot Strips,” NIST Memorandum, National Institute of Standards and Technology, May 15, 2008.

[12] L-Y. Cheng, “Heat Conduction in a NBSR Fuel Plate – Effect on Wall Heat Flux,” BNL Memorandum, Brookhaven National Laboratory, April 6, 2010.

[13] S. Cowell, W. B. Wilson, A. C. Hayes, P. Moller, and T. R. England, “A Manual for CINDER90 Version 07.4 Codes and Data,” LA-UR-07-8412, Los Alamos National Laboratory, March 2008.

[14] E. H. Wilson, “Irradiation Experiment Conceptual Design Parameters, Revision 1 End of June Submittal,” Electronic mail communication, Argonne National Laboratory, April 22, 2013.

[15] A. Cuadra and L. Y. Cheng, “Statistical Hot Channel Analysis for the NBSR,” BNL Technical Report, Brookhaven National Laboratory, to be published May 2014.

[16] Specification for Aluminum Clad Fuel Elements for the National Bureau of Standards Reactor, NCNR-ACFESpec-01, Rev. 5, September 3, 2010.

[17] “Specification for Low Enriched Uranium Monolithic Fuel Plates,” SPC-1635, Idaho National Laboratory, August 16, 2013.

[18] N.E. Woolstenhulme, “DDE-NBSR Status Report of Conceptual Design Activities,” INL/EXT-12-27079, Idaho National Laboratory, September 2012.

[19] J. Rest, *et al*, *U-Mo Fuels Handbook, Version 1.0,* RERTR Program, Argonne National Laboratory, June 2006.

[20] D. E. Burkes, G. S. Mickum, and D. M. Wachs, *Thermophysical Properties of U-10Mo Alloy*, INL/EXT-10-19373, November 2010.

[21] National Bureau of Standards, “Addendum 1 Final Safety Analysis Report on the National Bureau of Standards Reactor,” *NBSR 9 Addendum 1*, November 1980.

[22] National Bureau of Standards, “Final Safety Analysis Report on the National Bureau of Standards Reactor,” *NBSR 9*, April 1966.

[23] M. Gazit, “Accuracy of Measurements,” Email to L-Y. Cheng, National Institute of Standards and Technology, July 31, 2002.

[24] M. Kaminaga, K. Yamamoto, Y. Sudo, "Improvement of Critical Heat Flux Correlation for Research Reactors using Plate-Type Fuel*," J. Nucl. Sci. Technol. 35[12],* 943-951, 1998.

[25] P. Saha and N. Zuber, "Point of Net Vapor Generation and Vapor Void Fraction in Subcooled Boiling," Proc. 5th Int. Heat Transfer Conf., Vol. IV, p. 175, Tokyo, Japan, September 3-7, 1974.